Impact of Lunar and Solar Tides on Earth's Climate:Atmospheric Dynamics and Predictive Modeling

Abstract

The threat of climate change represents a significant challenge for a considerable proportion of the global population, due to the potential for disasters that it poses. Consequently, it is imperative to conduct comprehensive research on this subject. The objective of this study is to examine the influence of the Moon and Sun on atmospheric tides, the celestial bodies heights and their subsequent impact on temperature, wind distribution and precipitation. A model was developed and verified through satellite observations to assess its predictive capacity for climatic phenomena. The findings indicate that the heights of the moon and sun give rise to tidal phenomena that exert a significant climatic influence, which should not be disregarded. Prioritising the study of these phenomena will facilitate a deeper comprehension of the distribution of atmospheric high tides on Earth, which in turn will enable a more accurate prediction of wind patterns, temperatures and precipitation. This will in turn lead to the prevention of climatic disasters.

Keywords: Climate change, Atmospheric tides, Celestial body heights, Precipitation, Winds, Temperatures

LIST OF SYMBOLS

Δu_c: − − − − − − − − − − − − − − − − **Variation vitesse critique**

k_c: − − − − − − − − − − − − − − − − **Critical wavenumber**

h_{fluidT}: − − − − − − − − − − − − − − − − **Total fluid tide height**

g: − − − − − − − − − − − − − − − − $9,81 m/s^2$

G: − − − − − − − − − − − − − − − − **Gravitation constant**

u_i—: − − − − − − − − − − − − − − − − **Layer i speed**

χ_i: − − − − − − − − − − − − − − − − $(\vec{OP}_i, \vec{OM}_i)$

ρ_i: − − − − − − − − − − − − − − − − **Layer i density**

γ: − − − − − − − − − − − − − − − − **Surface tension coefficient**

k: − − − − − − − − − − − − − − − − **Angular wave number**

R: − − − − − − − − − − − − − − − − **Earth radius**

Δ: − − − − − − − − − − − − − − − − **The distance between the centre of the Earth and that of an extraterrestrial object is defined as the Earth-aster distance.**

a: − − − − − − − − − − − − − − − − $(\vec{ZS}, \vec{ZO})$

h: − − − − − − − − − − − − − − − − **Celestrial body heigth**

H: − − − − − − − − − − − − − − − − **Angle APZ angle PZA complement of the azimuth**

δ: − − − − − − − − − − − − − − − − **Declination**

I. INTRODUCTION

The phenomenon of climate change is a consequence of alterations in the composition of the atmosphere. This disruption to the atmospheric equilibrium is manifested in the form of an increase in the mean global temperature, which in turn gives rise to modifications in the physical, chemical and biological characteristics of the Earth system [1]. The environmental impacts are numerous, significant and increasingly frequent, including droughts, glacial and sea ice melting, rising sea levels and an increase in the frequency of tropical storms. These effects are felt by the entire global population and have a significant impact on biodiversity. Human-induced climate change is already affecting many weather and climate extremes in every region across the globe. Scientists are also observing changes across the whole of Earth's climate system; in the atmosphere, in the oceans, ice floes, and on land. Many of these changes are unprecedented, and some of the shifts are in motion now, while some - such as continued sea level rise – are already 'irreversible' for centuries to millennia, ahead, the report warns.But there is still time to limit climate change, IPCC experts say. Strong and sustained reductions in emissions of carbon dioxide (CO2) and other greenhouse gases, could quickly make air quality better, and in 20 to 30 years global temperatures could stabilize. Greenhouse gases are naturally present in the atmosphere. These gases form a layer around the Earth, which enables it to retain heat energy. This phenomenon is known as the greenhouse effect. Solar radiation heats the Earth, which then emits some of its heat back into space. The greenhouse gases present in the atmosphere serve to trap a portion of the heat emitted by the Earth, preventing its escape back into space. This phenomenon enables the maintenance of average planetary temperatures of $15C$. In the absence of this phenomenon, the temperature would be approximately $-18C$, which would not support the existence of life as we know it (Environment Canada, 2009). The rate of ice melting has increased markedly over the past 15 years. The extensive melting of ice results in an increase in the mass of water, which in turn causes a rise in sea levels. The projected increase in sea level is estimated to range between 9 and 88 centimetres between 1990 and 2100. This situation will have deleterious consequences for low-lying coastal areas, which are home to a significant proportion of the global population. In 2008, climate-related disasters resulted in the displacement of 20 million people (IOCHA and IDMC, 2009).

Furthermore, the availability of drinking water is likely to be impacted. As an illustration, an increase in temperature could result in a significant reduction in the water level of the Great Lakes,

due to enhanced evaporation. In addition to being a principal tributary of the St. Lawrence River, the Great Lakes represent the world's largest source of fresh water. A reduction in the quantity of drinking water could have significant implications(Environment Canada, 2002). Furthermore, the quality of lake water will require monitoring, as the proliferation of blue-green algae could intensify in the context of climate change. The phenomenon of climate change is already resulting in disruption to precipitation patterns. Such upheavals will be accompanied by an increase in the frequency and intensity of extreme weather events, including droughts, floods, heatwaves, heavy and abundant precipitation, and tornadoes. Such meteorological occurrences, frequently the catalyst for disasters, may well become more prevalent in the future (Environment Canada, 2008). In Quebec, projections indicate a potential increase in precipitation of up to 25 percent in the spring and 32 percent in the winter by 2050 (Bourque, Simonet, 2007). Notwithstanding these projections, the rate of snow cover in our winters remains uncertain, as precipitation may also manifest as rain. The majority of scientists now acknowledge that climate change will have significant implications for human health. In Canada, a number of health impacts have been identified, including an increase in respiratory diseases such as asthma, skin cancers, malaise and deaths linked to intense heat (Health Canada, 2008). Furthermore, climate change can exacerbate the phenomenon of heat islands in urban areas (Giguère, 2009), which has a range of health impacts, from heat cramps to heat syncope, and from heat exhaustion to heat stroke (Denis, 2010). Furthermore, an increase in vector-borne diseases is to be anticipated. With regard to the agricultural sector, climate change may exert a dual impact, both positive and negative. In general, an increase in average temperatures and a lengthening of the growing season should result in an increase in crop yields. Similarly, these changes should facilitate the production of crops that are adapted to higher temperatures (Bélanger, 2002). Conversely, the winter protection provided by snow cover for perennial crops may be adversely affected by milder winters with less snow. Furthermore, milder autumns may result in suboptimal conditions for hardening and potentially exacerbate damage to forage plants (Bélanger, 2002). The risk of invasion by insect pests could increase, and the distribution of species could change over the next few years as a result of more favourable climatic conditions (Roy, 2002). For example, observations have confirmed an increased likelihood of invasion by the western rootworm and the leafroller. For example, observations have confirmed that the western rootworm and the oriental fruit moth, which were previously present in southern Quebec, are now exhibiting a northward migration. The occurrence of specific insect species is now being documented over a more extended period, necessitating the initiation of surveillance activities at

an earlier stage in the season. The expansion of weed habitats is also likely to occur as a result of the favourable conditions brought about by climate change. Furthermore, some studies have indicated that weeds may possess greater adaptive capacity to climate change than crops (Ziska, undated). It is imperative that the agricultural sector adapt to the new conditions brought about by climate change. It is evident that the agricultural sector will face significant challenges in the coming years. However, there are opportunities for farmers to adapt to climate change by introducing new crop varieties or new types of production, ensuring better soil protection and improved water conditions. The earlier agricultural producers are made aware of the necessary adaptations to be made in order to mitigate the negative impact of climate change on their farms, the more effectively they will be able to implement these changes. Indeed, the implementation of measures to combat climate change at this juncture is more advantageous than the requisite adaptations that will be necessitated by the impacts. The advancement of scientific research has led to a notable evolution in our understanding of the climate. In light of the knowledge acquired since the signing of the Kyoto Protocol in 1997, climate scientists have posited that countries' targets will have to be revised upwards. A temperature rise in excess of 2°C could precipitate significant climate disruption on a global scale, with the potential for major humanitarian and political crises to ensue. In order to take effective action against global warming, it is essential to ascertain whether greenhouse gases are indeed the primary cause. In order to address this question, this study will also investigate the impact of the position of stars such as the Sun and the Moon on atmospheric tidal phenomena and climate consequences [2][3] [4]. This will be done with a view to comparing the two models and deducing which of the two points of view has the greatest real impact on climate change.

II. METHODS

In the local reference frame, only the zenith angle and the height can be accurately measured to determine the latitude and local time. The objective is to derive the formulae that enable the height of a star to be related to values of position and time. [5] The celestial sphere, or sphere of fixed points, is linked to the equatorial coordinate system (right ascension and declination). The observer is located in two reference frames related to their position: the local reference frame (azimuth and height) and the hourly reference frame (hourly angle and declination). The observer is situated within two distinct reference frames, both of which are related to their position[6]. The

first of these is the local reference frame, which encompasses azimuth and height. The second is the time reference frame, which incorporates time angle and declination [7]. These two reference frames are specific to the location. The relationship with the sphere of fixed points, which rotates for the observer, is the transition from the time system to the equatorial system by sidereal time TS, utilising the elementary relationship [8]. The relation with the sphere of fixed stars, which rotates for the observer, is the passage from the hourly system to the equatorial system by sidereal time TS, by the elementary relation :

$$H = TS - \alpha \tag{1}$$

. The transition between the local reference frame and the time reference frame can be conceptualised as a mere change of coordinates (see Figure 1).

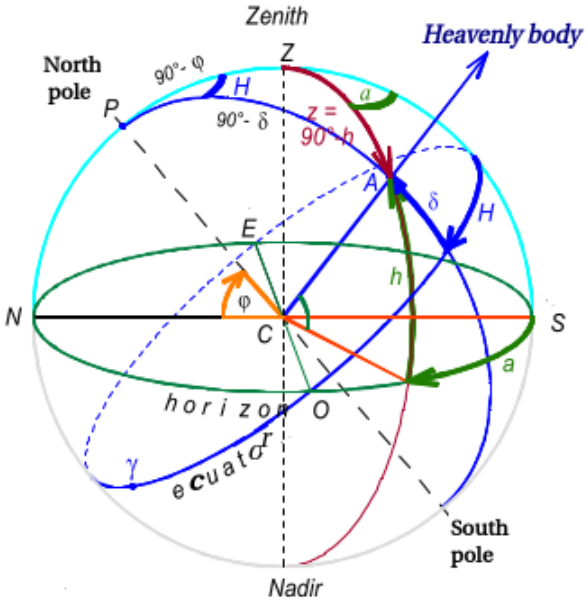

FIG. 1. Coordinates

• **horizontal coordinates ⇒ time coordinates:**

$$sin\delta = sin\varphi.cosz - cos\varphi.sinz.cosa \tag{2}$$

$$cos\delta.sinH = sinz.sina \tag{3}$$

$$cos\delta.cosH = cos\varphi.cosz + sin\varphi.sinz.cosa \tag{4}$$

• **Time coordinates ⇒ horizontal coordinates:**

$$cosz = sin\varphi.sin\delta - cos\varphi.cos\delta.cosH \tag{5}$$

$$sinz.sina = cos\delta.sinH \tag{6}$$

$$sinz.cosa = -cos\varphi.sin\delta + sin\varphi.cos\delta.cosH \tag{7}$$

The complement of the height is found by using the latitude of the location, denoted by φ, and the zenith distance, denoted by z [9]. In the figure opposite, all these coordinates are found in the miracle triangle AZP:

- angle APZ hour angle
- angle PZA complement of the azimuth
- arc PA or angle PCA: declination supplement
- arc ZA or angle ZCA: complement of height
- arc PZ or angle PCZ: latitude complement

The formula for the PZA triangle is as follows (see Figure 2)

$$cosZA = cosPA.cosPZ + sinPA.sinPZ.cosH \tag{8}$$

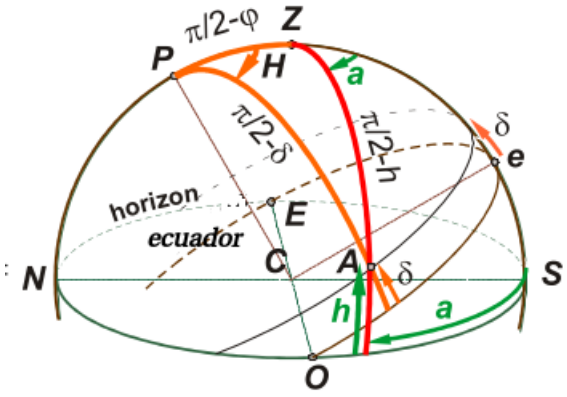

FIG. 2. PZA Triangular

$$sinh = sin\delta.sin\varphi + cos\delta.cos\varphi.cosH \tag{9}$$

$$cosH = \frac{sinh - sin\delta.sin\varphi}{cos\delta.cos\varphi} \tag{10}$$

Using the sine formula, we obtain the azimuth:

$$\frac{sina}{cos\delta} = \frac{sinH}{cosh} \tag{11}$$

With

$$sina = \frac{sinH.cos\delta}{cosh} \tag{12}$$

The heights of the Moon and the Sun are not fixed throughout the year (see Figure 5); rather, they vary continuously each day, which generates tidal phenomena on the fluids (liquids (water reservoirs), gases (atmosphere)) on the surface of the Earth[10].

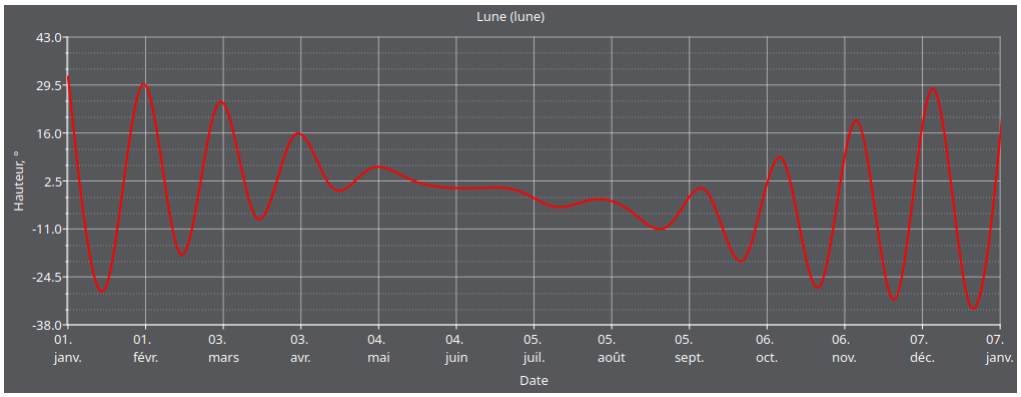

FIG. 3. Variations in the height of the Moon during 2024

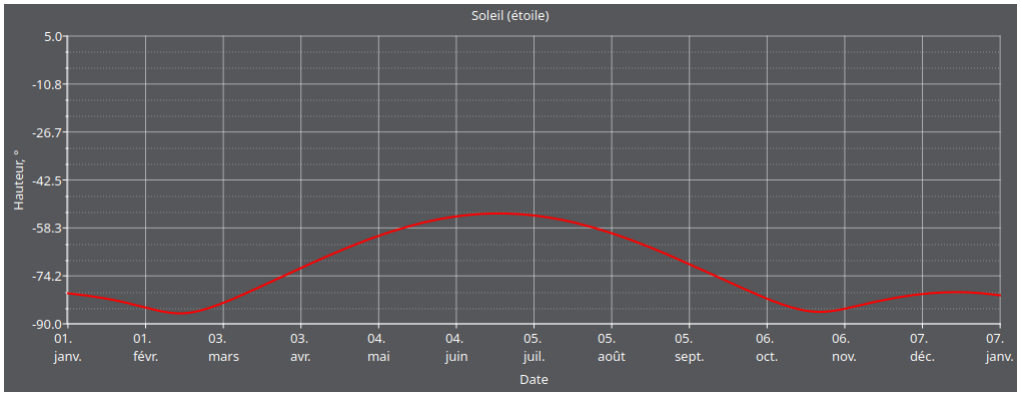

FIG. 4. Variations in the height of the Sun during 2024

These tidal phenomena elucidate the movements of the Earth's fluids, which play a foundational role in the climate of planet Earth (see Figure 6 and Figure 7). The following figures illustrate the displacement of the disruptive star [11].

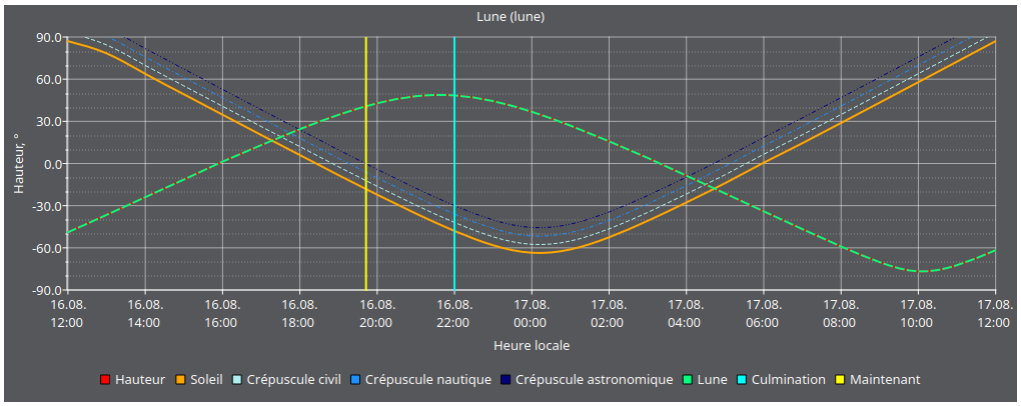

FIG. 5. Variations in the height of the Moon and the Sun on 23/10/2024

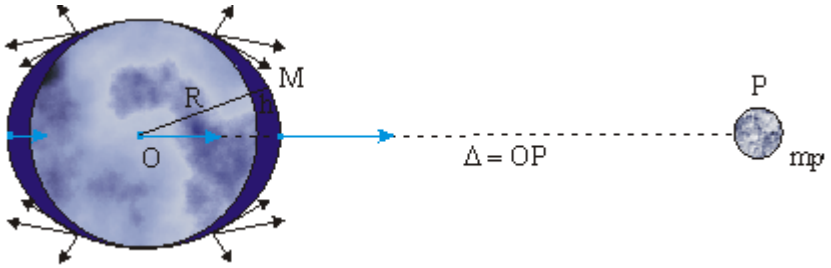

FIG. 6. The disruptive body in the earth equator

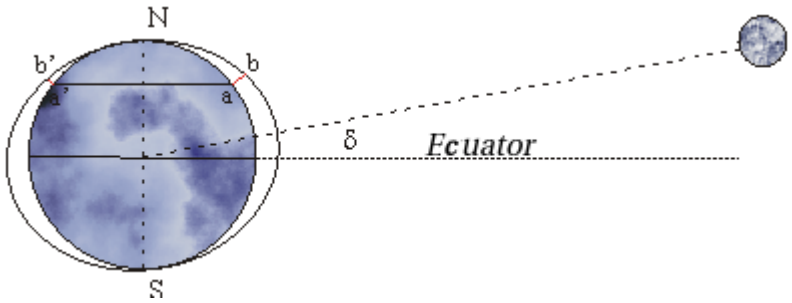

FIG. 7. The perturator body is not on the Earth's equator

The tidal height is given by the following formula as a function of the star i (Sun, Moon, etc.):

$$h_{fluidi} = \frac{Gm_{pi}R^2}{2g\Delta}(3cos^2\chi_i - 1) \tag{13}$$

$$h_{fluidT} = \sum_i \frac{Gm_{pi}R^2}{2g\Delta}\{3cos^2[cos^{-1}(\frac{sinh_i - sin\delta_i.sin\varphi_i}{cos\delta_i.cos\varphi_i})] - 1\} \tag{14}$$

• h_{fluidT} : total height of the fluid tide

• g : $9,81 m/s^2$

•G: gravitational constant $G = 6.67259 * 10^{-11} m^3 kg^{-1} s^{-2}$

•χ_i: $(\vec{OP_i}, \vec{OM_i})$

In these tidal movements, shear due to Kelvin-Helmholtz instabilities is generated, playing a crucial role in the speeds and forces of the harmathan and the monsoon. Kelvin-Helmholtz instabilities are caused by a shear phenomenon which can occur in a single fluid (due to a velocity gradient in the normal direction). Such instabilities may occur in a single fluid (due to a velocity gradient in the direction normal to that of the flow), or at the interface between two superimposed fluids moving at different speeds. These instabilities manifest as self-coiling vortices [12]. They can, in rare instances, be observed at the summit of specific clouds on Earth, designated as fluctus clouds. Additionally, Kelvin-Helmholtz instabilities manifest in the upper atmosphere of gas giants, where they are driven by the disparity in velocity between the jet streams that form parallel bands to the equator of these planets. We may consider a problem in which two layers of identical height, h, comprising immiscible fluids, are superimposed and separated by an interface in the presence of surface tension and in a gravitational field. The theoretical study of the Kelvin-Helmholtz instability is conducted through a linear stability analysis of the problem, which enables the determination of a dispersion relation. Subsequently, the dispersion relation is employed to ascertain the requisite condition for a wave number k to be unstable [13].

$$(u_1 - u_2)^2 > \frac{\rho_1 + \rho_2}{\rho_1 \rho_2} [\gamma k + (\rho_1 - \rho_2)\frac{g}{k}] tanh(k h_{fluidT}) \tag{15}$$

$$(u_1 - u_2)^2 > \sum_i \frac{\rho_1 + \rho_2}{\rho_1 \rho_2} [\gamma k + (\rho_1 - \rho_2)\frac{g}{k}] tanh(k \frac{G m_{pi} R^2}{2g\Delta} \{3cos^2[cos^{-1}(\frac{sinh_i - sin\delta_i . sin\varphi_i}{cos\delta_i . cos\varphi_i})] - 1\}) \tag{16}$$

with u following this equation[14]:

$$u(r \in \{x,y,z\}) = [\lambda^2 \alpha \sum_{n=1}^{+\infty} \frac{[2(\lambda r - \frac{t}{\tau_c})]^n}{2n!} - (N-10) \sum_{n=1}^{+\infty} \sum_{j=1}^{+\infty} \frac{(500n+2)^{j-1}}{n! j! (500n+1)} (\lambda r - \frac{t}{\tau_c})^j + \lambda^2 \frac{f r^2}{2} - \lambda^2 \frac{Pr}{\rho}] \frac{\tau_c}{\omega^2 t} + \frac{\lambda^2 \tau_c}{t} \int \sum_{n=1}^{+\infty} \frac{(\lambda r^{1-n} - \frac{t r^{-n}}{\tau_c})^n}{n!} dr \tag{17}$$

Using indices 1 and 2 for the upper and lower layers respectively and denoting γ the surface tension coefficient and k the (angular) wavenumber, defined from the wavelength λ by $k = 2\pi/\lambda$. The case of Rayleigh-Taylor instability is found in the absence of surface tension if $rho_1 > \rho_2$ [15]. All the wavenumbers are then unconditionally unstable (the condition is verified whatever

the value of k since the left-hand member is positive or zero and the right-hand member is strictly negative). The wavenumber function, represented by the variable k, reaches a minimum on the right-hand side of Equation (16) at the critical wavenumber, k_c. This allows the critical value of the velocity difference, u_c, to be determined, beyond which the Kelvin-Helmholtz instability can develop. In the event that the velocity difference is less than the aforementioned critical value, all wave numbers are deemed to be stable[16]. In all other cases, a range of values for k are unstable, resulting in the development of Kelvin-Helmholtz instabilities. Initially, these instabilities manifest linearly, but then undergo a rapid transition to a nonlinear state at the interface [17]. The critical wave number and the critical velocity difference are given by the following equations:

$$k_c = \sqrt{\frac{g(\rho_2 - \rho_1)}{\gamma}} \tag{18}$$

$$\Delta u_c = (2\frac{\rho_1 + \rho_2}{\rho_1 \rho_2}\sqrt{g(\rho_2 - \rho_1)\gamma})^{1/2} \tag{19}$$

Chandrasekhar gives more details concerning Kelvin-Helmholtz instabilities. The experimental apparatus employed by Thorpe (see Figure 8) provides an excellent opportunity to study the development of Kelvin-Helmholtz instabilities, which occur in a sheared flow at the interface between two immiscible fluids [17]. Our main results are deduced from climate sattelite oservations.

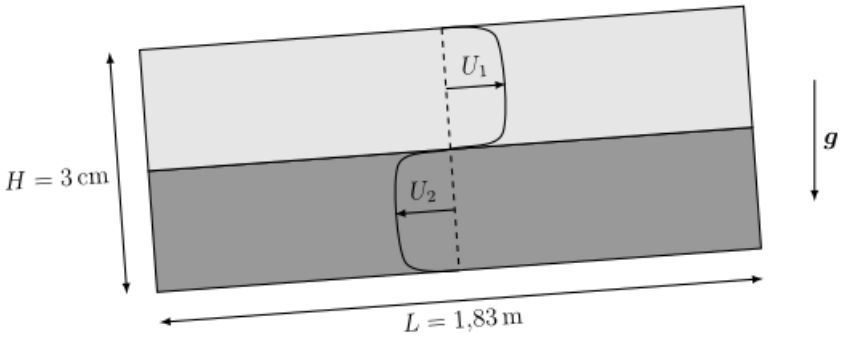

FIG. 8. Thorpe's experiment

III. RESULTS AND DISCUSSION

The initial observations on meteblue sattelite software,on atmospheric tide phenomena indicate that the degree of chaos observed in the atmospheric layer is contingent upon the density of the atmospheric layer in question. For high atmospheric tides, the chaos is observed at the higher levels of the atmospheric layer, while for low atmospheric tides, the chaos is observed at the lower levels of the atmospheric layer (see Figure 9). It can thus be observed that between zones of

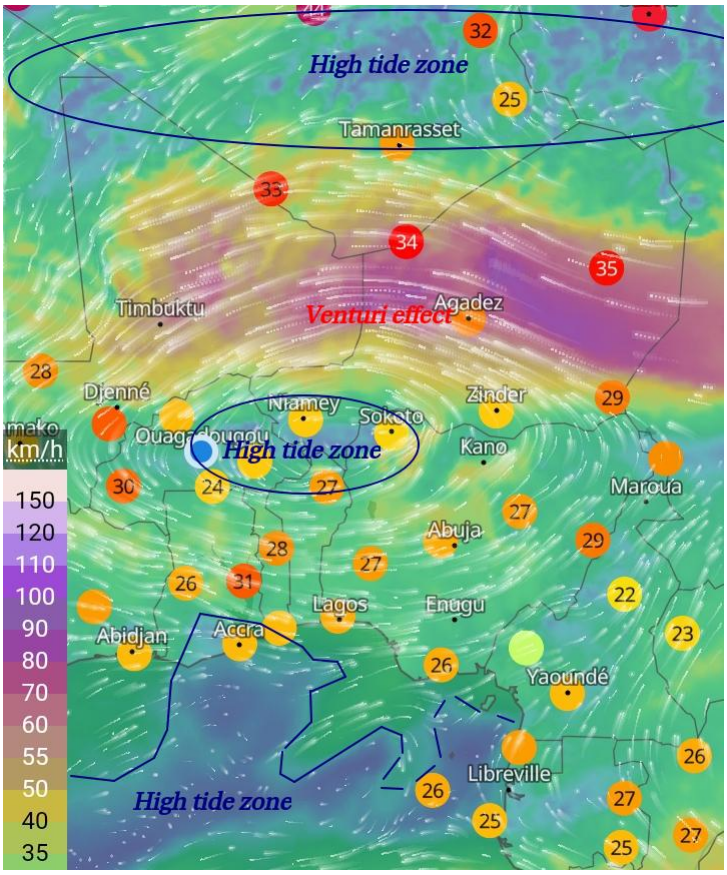

FIG. 9. Venturi effect in an atmospheric zone

high tide, the winds flow in accordance with the Venturi effect, resulting in an acceleration of the winds within this atmospheric domain and, consequently, an influence on the distribution of temperatures, winds and precipitation over the planetary zone in question (see Figure 10).

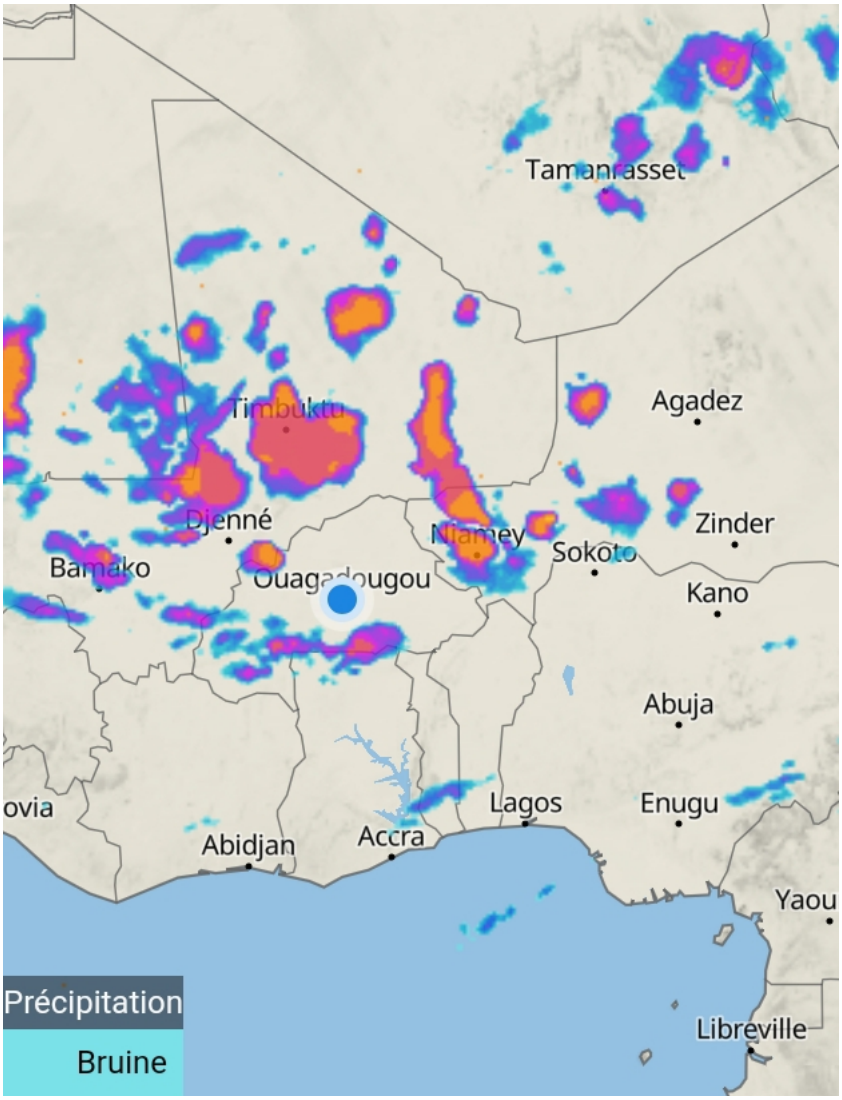

FIG. 10. Influence on oragic formations on the observed planetary domain

Further satellite observations were conducted to gain further insight into the formation of these expansive clouds. These observations demonstrate that each layer possesses a distinct density resulting from the accumulation of gases at varying heights. The consequences of this is that wind speed in a specific direction within an atmospheric layer gives rise to the circulation of adjacent layers in the opposite direction, as a result of Kelvin-Helmholtz instabilities (see Figure 11).

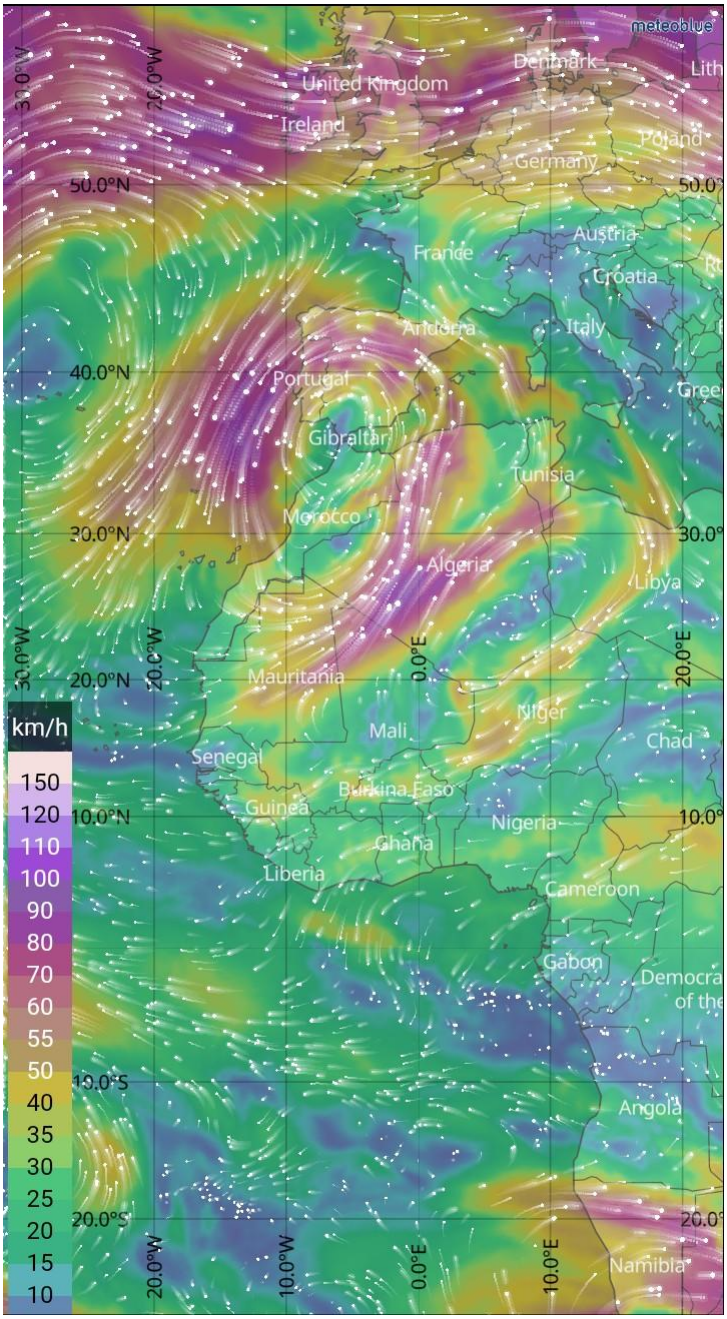

FIG. 11. Wind circulation at an altitude of 700Mo

As a consequence of the Earth's surface insolation, the planet's temperature rises, thereby acting as a heat source for the surrounding atmosphere. As the air temperature increases, it expands and, as a consequence of this expansion, its density is reduced. The circulation of cold winds, caused by atmospheric tides above the given area, results in an upward suction in the opposite direction due to Kelvin-Helmholtz instabilities of the warm air at low altitudes near the ground. This leads to the formation of a circulation. As the air warms, it is able to absorb more water,

which in turn causes a cooling effect and the gradual disappearance of humidity. This results in the formation of clouds at higher altitudes. Noted that once reach the 700Mo altitude, they are carried by this layer winds (see Figure 12).

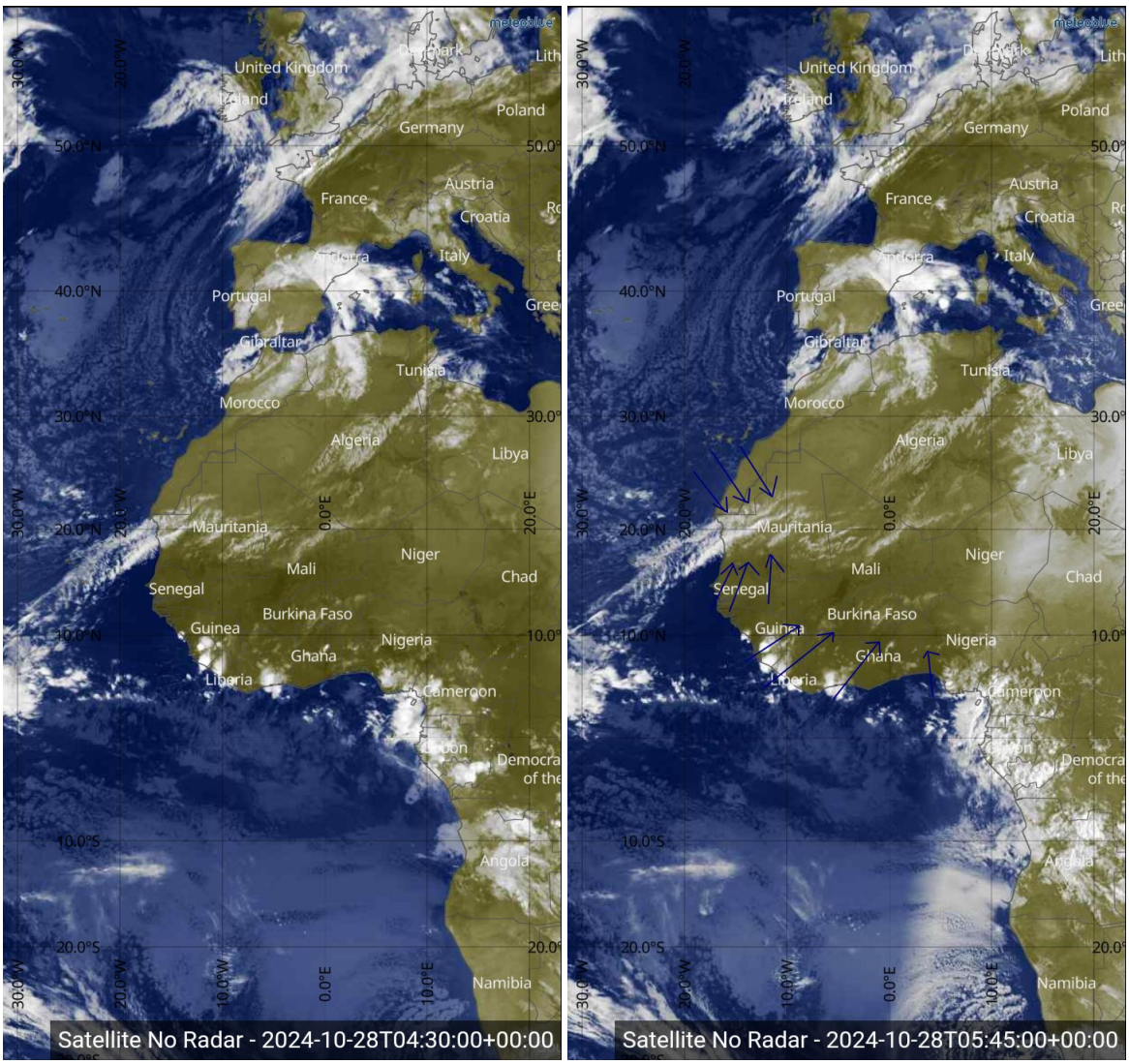

FIG. 12. Movement in the opposite direction to the winds of the lower atmospheric layers, which are charged with water vapour, occurs as the vapour condenses.

Specific case study and zone rainfull function

The following figures illustrate the distribution of temperatures, precipitation and winds in Ouagadougou as a function of the heights of the Moon and Sun for a period from May to September

2024 (see Figure 14 in appendix).

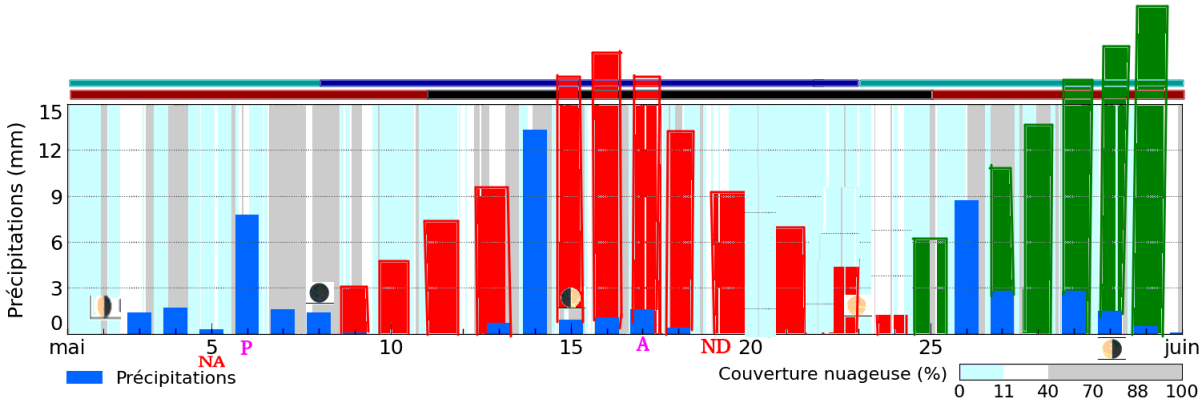

FIG. 13. Gaussian rain distriution

Figure 13, shows blues bars for rainfall obtained during the months, reds and greens bars that must be ut wasn't. To explain this, suppose that during the rainy month in the zone, four(4) Gaussian rainfall functions must be taing into account and over the months studied:

$$P_i = \frac{P_{imax}}{\sigma_i\sqrt{2\pi}} exp[-\frac{1}{2}(\frac{x-\mu_i}{\sigma_i})^2] cos^2(\phi_i) \tag{20}$$

- $cos^2\phi_i$: Giving the daily water distribution during the Moon increasing, decreasing, rising setting activities period.

- $\frac{P_{imax}}{\sigma_i\sqrt{2\pi}} exp[-\frac{1}{2}(\frac{x-\mu_i}{\sigma_i})^2]$: Moon activity period gaussian.

99 percent of Moon activity period is in $[x-3\sigma_i, x+3\sigma_i]$.To get a best rainfall prediction, we need to take into- account the Moon activity days interval corresponding to increasing, decreasing, rising and setting Moon. The general prediction is define as

$$\begin{aligned} P_M = &\frac{P_{Imax}}{\sigma_I\sqrt{2\pi}} exp[-\frac{1}{2}(\frac{x-\mu_I}{\sigma_I})^2] cos^2(\phi_I) - \frac{P_{Smax}}{\sigma_S\sqrt{2\pi}} exp[-\frac{1}{2}(\frac{x-\mu_S}{\sigma_S})^2] cos^2(\phi_S) \\ &- \frac{P_{Dmax}}{\sigma_D\sqrt{2\pi}} exp[-\frac{1}{2}(\frac{x-\mu_D}{\sigma_D})^2] cos^2(\phi_D) + \frac{P_{Rmax}}{\sigma_R\sqrt{2\pi}} exp[-\frac{1}{2}(\frac{x-\mu_R}{\sigma_R})^2] cos^2(\phi_R) \end{aligned} \tag{21}$$

μ_i, σ_i, ϕ_i, Smax, Dmax,Imax, Rmax are constants to be determined. The **TOUGMA's climate model** is summarize as follow:

$$\left\{\begin{array}{l} u(r\in\{x,y,z\}) = [\lambda^2\alpha\sum_{n=1}^{+\infty}\frac{[2(\lambda r-\frac{t}{\tau_c})]^n}{2n!} - (N-10)\sum_{n=1}^{+\infty}\sum_{j=1}^{+\infty}\frac{(500n+2)^{j-1}}{n!j!(500n+1)}(\lambda r-\frac{t}{\tau_c})^j + \lambda^2\frac{fr^2}{2} - \lambda^2\frac{Pr}{\rho}]\frac{\tau_c}{\omega^2 t} \\ +\frac{\lambda^2\tau_c}{t}\int\sum_{n=1}^{+\infty}\frac{(\lambda r^{1-n}-\frac{tr^{-n}}{\tau_c})^n}{n!}dr \\ \\ (u_1-u_2)^2 > \sum_i\frac{\rho_1+\rho_2}{\rho_1\rho_2}[\gamma k+(\rho_1-\rho_2)\frac{g}{k}]tanh(k\frac{Gm_{pi}R^2}{2g\Delta}\{3cos^2[cos^{-1}(\frac{sinh_i-sin\delta_i.sin\varphi_i}{cos\delta_i.cos\varphi_i})]-1\}) \\ \\ P_M = \frac{P_{Imax}}{\sigma_I\sqrt{2\pi}}exp[-\frac{1}{2}(\frac{x-\mu_I}{\sigma_I})^2]cos^2(\phi_I) - \frac{P_{Smax}}{\sigma_S\sqrt{2\pi}}exp[-\frac{1}{2}(\frac{x-\mu_S}{\sigma_S})^2]cos^2(\phi_S) - \frac{P_{Dmax}}{\sigma_D\sqrt{2\pi}}exp[-\frac{1}{2}(\frac{x-\mu_D}{\sigma_D})^2]cos^2(\phi_D) \\ +\frac{P_{Rmax}}{\sigma_R\sqrt{2\pi}}exp[-\frac{1}{2}(\frac{x-\mu_R}{\sigma_R})^2]cos^2(\phi_R) \end{array}\right\}$$

IV. CONCLUSION AND FUTURE WORK

In this study atmospheric tides generated by the heights of the moon and the sun has a considerable impact on the climate, which should not be overlooked. It is imperative that these phenomena be accorded priority in the study of climatic phenomena on planet Earth. The alteration in air density resulting from the accumulation of gases produced by human activity and solar storm generated by sun activities exerts an influence on the distribution of atmospheric high tides across the planet, which in turn affects the distribution of winds, temperatures and precipitation. The main climate change is the atmospheric tides due to Sun and Moon height. However, greenhouse gases have an impact on atmospheric layers density and the distribution and volume of these atmospheric tides. This work encourages a deeper comprehension of the dispersion of elevated atmospheric tides in both time and space, with the objective of developing more accurate forecasts and, consequently, the prevention of potential climatic catastrophes that could have adverse effects on populations. A deeper comprehension of this distribution will facilitate a more accurate assessment of the actual impact of anthropogenic greenhouse gases on the climate. This, in turn, will prove invaluable in formulating effective climate change mitigation strategies that will benefit humanity.

V. APPENDIX

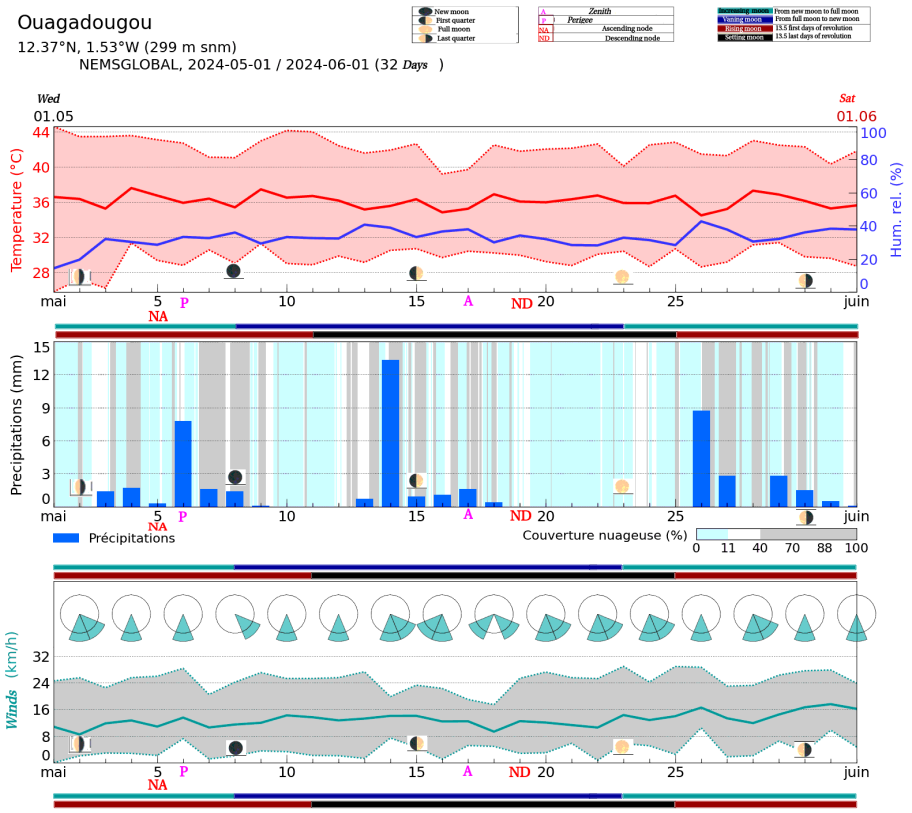
Ouagadougou
12.37°N, 1.53°W (299 m snm)
NEMSGLOBAL, 2024-05-01 / 2024-06-01 (32 Days)
New moon
First quarter
Full moon
Last quarter
Zenith
Perigee
Ascending node
Descending node
Waxing moon
Waning moon
Rising moon
Setting moon
From new moon to full moon
From full moon to new moon
13.5 first days of revolution
13.5 last days of revolution
Wed 01.05
Sat 01.06
Temperature (°C)
Hum. rel. (%)
Precipitations (mm)
Précipitations
Couverture nuageuse (%)
Winds (km/h)
mai
juin

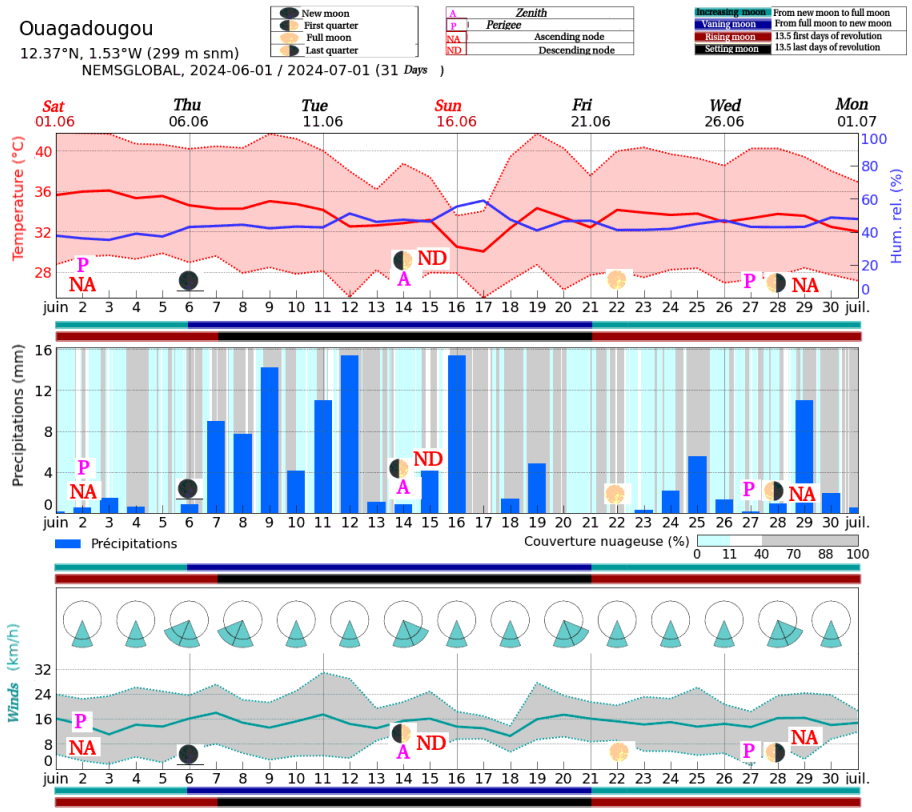
Ouagadougou
12.37°N, 1.53°W (299 m snm)
NEMSGLOBAL, 2024-06-01 / 2024-07-01 (31 Days)
New moon
First quarter
Full moon
Last quarter
Zenith
Perigee
Ascending node
Descending node
Waxing moon
Waning moon
Rising moon
Setting moon
From new moon to full moon
From full moon to new moon
13.5 first days of revolution
13.5 last days of revolution
Sat 01.06
Thu 06.06
Tue 11.06
Sun 16.06
Fri 21.06
Wed 26.06
Mon 01.07
Temperature (°C)
Hum. rel. (%)
Precipitations (mm)
Précipitations
Couverture nuageuse (%)
Winds (km/h)
juin
juil.

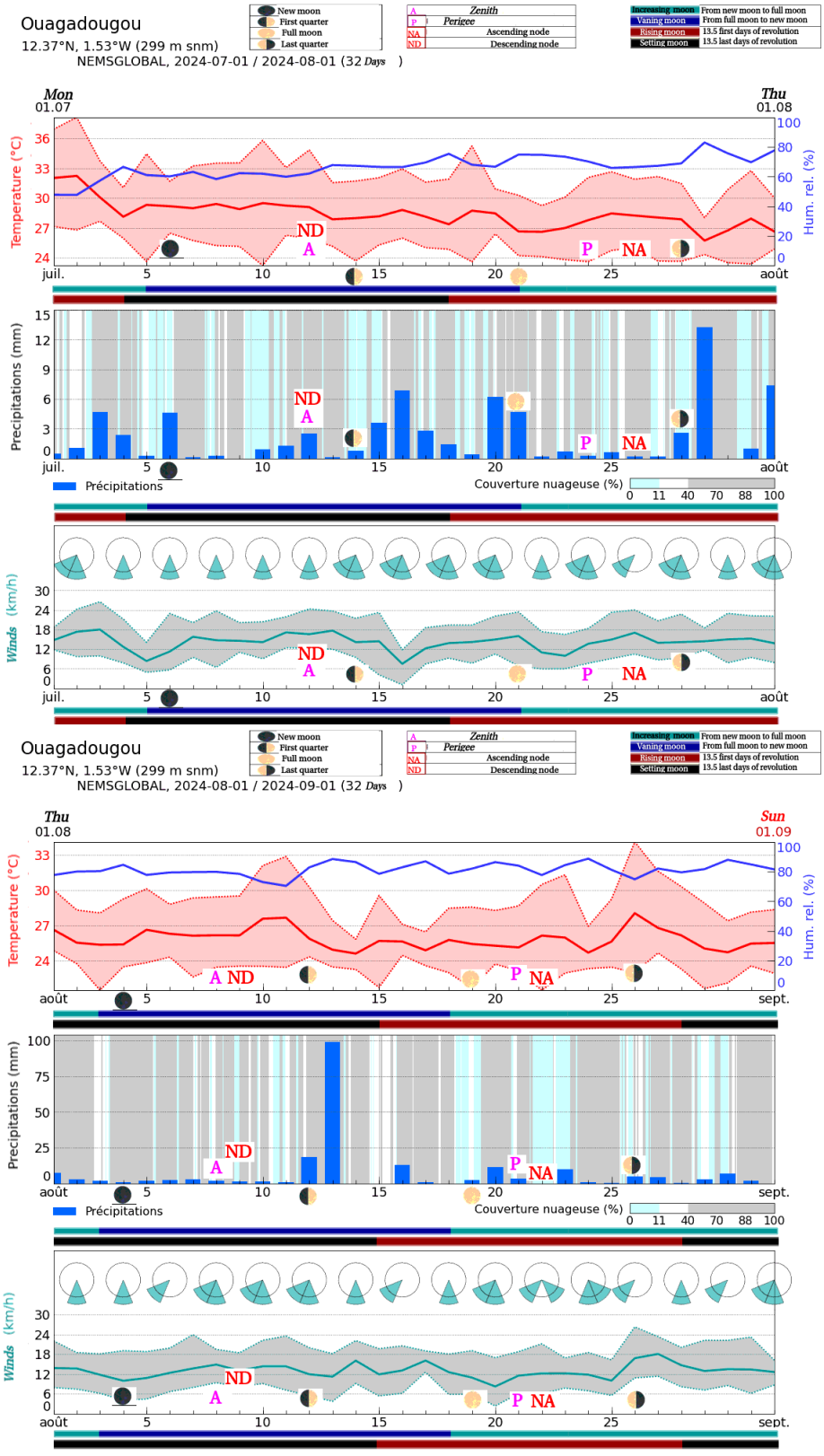
Ouagadougou
12.37°N, 1.53°W (299 m snm)
NEMSGLOBAL, 2024-07-01 / 2024-08-01 (32 Days)
New moon
First quarter
Full moon
Last quarter
A Zenith
P Perigee
NA Ascending node
ND Descending node
Increasing moon From new moon to full moon
Waning moon From full moon to new moon
Rising moon 13.5 first days of revolution
Setting moon 13.5 last days of revolution
Mon 01.07
Thu 01.08
Temperature (°C)
Hum. rel. (%)
Precipitations (mm)
Précipitations
Couverture nuageuse (%)
0 11 40 70 88 100
Winds (km/h)
juil.
août
ND
A
P
NA
Ouagadougou
12.37°N, 1.53°W (299 m snm)
NEMSGLOBAL, 2024-08-01 / 2024-09-01 (32 Days)
Thu 01.08
Sun 01.09
sept.

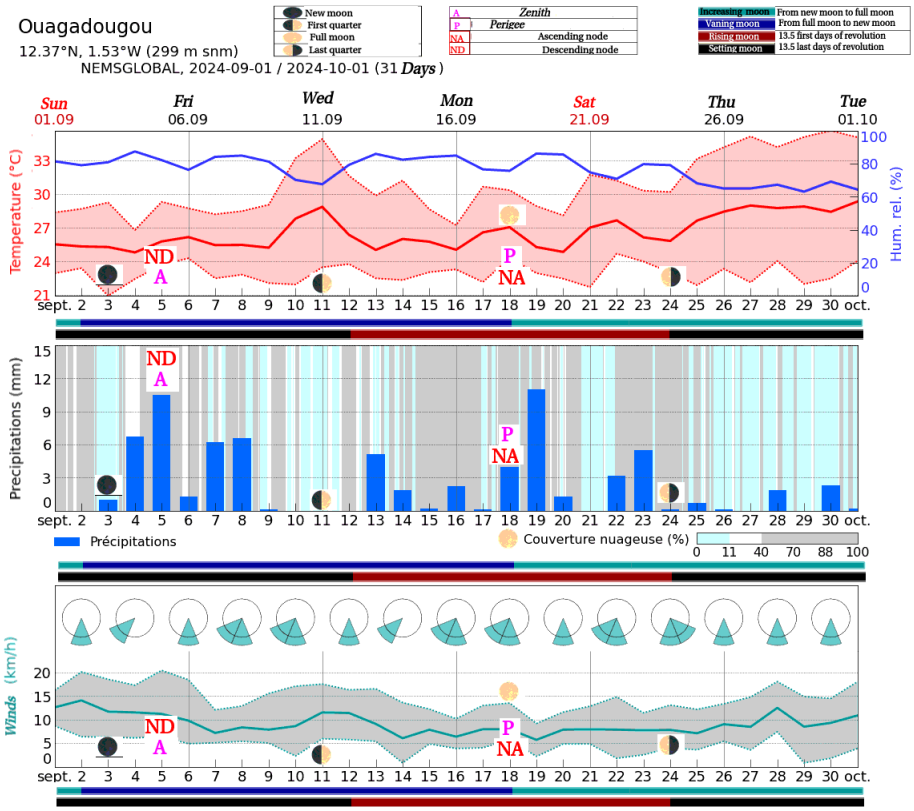

FIG. 14. Movement in the opposite direction to the winds of the lower atmospheric layers, which are charged with water vapour, occurs as the vapour condenses.

ACKNOWLEDGEMENTS

Funding and/or Conflicts of interests/Competing interests The present study received no financial aid from any government/non- government agency. And there is no conflicts of interests for this study.

REFERENCES

[1]M. C. J. Camirand C. Gingras, J. Camirand, "Les changements climatiques :quels en sont les causes et les impacts ?," *Nature Québec*, 2011.

[2]C. Covey and al, "Atmospheric tides in the latest generation of climate models," *Journal of the Atmospheric Sciences*, 2014.

[3]G. Stober, "Seasonal evolution of winds, atmospheric tides and reynolds stress components in southern hemisphere mesosphere/lower thermosphere in 2019," *Annales Geophysicae*, 2020.

[4]D. Panchera and al, "Global response of the ionosphere to atmospheric tides forced from below: Comparison between cosmic measurements and simulations by atmosphere-ionosphere coupled model gaia," *Open Journal of Geophysical Research Atmospheres*, 2012.

[5]J.-B. Denoville, "Le traité de navigation," *Manuscrit De La Bibliothèque Municipale De Rouen. . Ed. Point De Vues http://assprouen.free.fr/denoville*, .

[6]RECORD, "Documentation de l'université de strasbourg)http://num-scd-ulp.u-strasbg.fr:8080/640," *Etude des modifications induites au niveau de la composition des fumées et des cendres, 2001, 63 p, n°00-0219/1A.*, .

[7]., "Mémoire sur l'observation des longitudes en mer," *La Caille - MARS 1759, p63-99.*, 1759.

[8]., "Sur la recherche des longitudes en mer," *HARS, 1722, p 96-120.*, 1722.

[9]Lalande, "Usage des mouvements de la lune pour trouver la longitudes en mer," *Astronomie tome 3, 651-682,*, 1792.

[10]P. E., "Astronomie des marins," *sur Google books, mais planches scannées avec les planches repliées.*, 1766.

[11]H. et MARS, "Histoire et mémoires de l'académie royale des sciences," ., .

[12]S. Chandrasekhar, "Hydrodynamic and hydromagnetic stability.," *isbn : 978-0-48664-071-6.*, 1961.

[13]S. A. Thorpe, "Experiments on the instability of stratified shear flows: Immiscible fluids," *Journal of Fluid Mechanics, t. 39, no 1, p. 25-48, 1969. doi : 10.1017/s0022112069002023.*, 1969.

[14]J. L. W. TOUGMA, "Method of analytical resolution of the navier-stokes equations," *Open Journal of Fluid Dynamics*, 2023.

[15]E. B. D. V. et S. H. Davis, "On the motion of a fluid-fluid interface along a solid surface," *Journal of Fluid Mechanics, t. 65, no 1, p. 71-95, 1974. doi : 10.1017/s0022112074001261.*, 1974.

[16]L. F. S. et M. K. Gordon, "Computer solution of ordinary differential equations,the initial value problem," *isbn : 978-0-7167-0461-4.*, 1975.

[17]S. Skelboe, "The control of order and steplength for backward differentiation methods," *BIT, t. 17, no 1, p. 91-107, 1977. doi : 10.1007/bf01932401.*, 1976.